Research Square

Preprints are preliminary reports that have not undergone peer review.
They should not be considered conclusive, used to inform clinical practice,
or referenced by the media as validated information.

Fabrication of light trapping structures specialized for near- infrared light by nanoimprinting for the application to thin crystalline silicon solar cells

Yuto Kimata (kimata.yuto.w2@s.mail.nagoya-u.ac.jp)
Nagoya University
Kazuhiro Gotoh
Nagoya University
Satoru Miyamoto
Nagoya University
Shinya Kato
Nagoya Institute of Technology
Yasuyoshi Kurokawa
Nagoya University
Noritaka Usami
Nagoya University

Research Article

Keywords:

Posted Date: February 13th, 2023

DOI: https://doi.org/10.21203/rs.3.rs-2544646/v1

License: This work is licensed under a Creative Commons Attribution 4.0 International License.
Read Full License

Additional Declarations: No competing interests reported.

Version of Record: A version of this preprint was published at Discover Nano on May 3rd, 2023. See the published version at https://doi.org/10.1186/s11671-023-03840-6.

Abstract

Vehicle-integrated photovoltaics (VIPV) are gaining attention to realize a decarbonized society in the future, and the specifications for solar cells used in VIPV are predicated on a low cost, high efficiency, and the ability to be applied to curved surfaces. One way to meet these requirements is to make the silicon substrate thinner. However, thinner substrates result in lower near-infrared light absorption and lower efficiency. To increase light absorption, light trapping structures (LTSs) can be implemented. However, conventional alkali etched pyramid textures are not specialized for near-infrared light and are insufficient to improve near-infrared light absorption. Therefore, in this study, as an alternative to alkaline etching, we employed a nanoimprinting method that can easily fabricate submicron-sized LTSs on solar cells over a large area. In addition, as a master mold fabrication method with submicron-sized patterns, silica colloidal lithography was adopted. As a result, by controlling silica coverage, diameter of silica particles (D), and etching time (t_{et}), the density, height, and size of LTSs could be controlled. At the silica coverage of 40%, D = 800 nm, and t_{et}=5 minutes, the reduction of reflectance below 65% at 1100 nm and the theoretical short-circuit current gain of 1.55 mA/cm^2 was achieved.

Introduction

In recent years, VIPVs have attracted much attention to achieve carbon neutrality [1–4]. One approach to achieve long distances to drive is an implementation of highly efficient tandem solar cells on VIPVs. Schygulla *et al*. reported a two-terminal wafer-bonded III–V//crystalline Si (c-Si) triple-junction solar cell with the efficiency of 35.9% [5]. To implement solar cells on curved surfaces like a roof and hood of vehicles, solar cells should be flexible and a silicon substrate must be thin. Sai *et al*. fabricated a flexible Si heterojunction solar cell with a thickness of approximately 50 μm [6]. However, the challenge is that thin silicon substrates do not absorb near-infrared light well enough [7]. In general, alkaline etching [8] and photolithography [9, 10] have been used to fabricate optical confinement structures. However, the alkaline etching method is insufficient to absorb near-infrared light, and it is difficult to fabricate on thin silicon substrates and in a large area. Photolithography also has the problem of low throughput. There are some other approaches to enhance the near-infrared light absorption [11–14]. One of them is the nanoimprinting technique, which enables us to control the morphology of submicron-sized light trapping structures (LTSs) and to fabricate the LTSs on a thin Si substrate in a large area [14–23]. Various designs of LTSs have been fabricated by nanoimprinting, including a binary diffraction grating [19] and inverted pyramid shapes [20]. Although conventional LTSs fabricated by nanoimprinting technique are periodic, non-periodic LTSs will enhance light absorption in a wide wavelength range. For example, conventional random pyramid texture for c-Si solar cells [8] and ZnO texture structure for Si-based or chalcopyrite thin film solar cells [24, 25] are reported.

In this study, to obtain non-periodic LTSs, the fabrication of master molds by colloidal lithography using silica particles [19] was combined with nanoimprinting. The colloidal lithography has the advantage of easily controlling the morphology of LTSs in a submicron range. The diameter and height of LTSs were

controlled by varying the diameter of silica particles (D) and etching time (t_{et}). The silica coverage was controlled by varying the concentration and deposition time of silica solution and spin-coating speed. We implemented the LTSs on the backside of c-Si/ITO substrates by nanoimprinting technique and evaluated the light confinement performance.

Experimental Methods

The fabrication process of a master mold of LTSs is shown in Fig. 1(a). A 2 × 2 cm^2 c-Si substrate was used. c-Si substrates were cleaned by the RCA process. Subsequently, they were immersed in 5% hydrofluoric acid for 1 minute to remove a natural oxide. The substrates were immersed in ethylenediamine and irradiated with UV light for 3 hours. After that, ethylenediamine was removed with toluene, ethanol, and deiozied (DI) water. Silica particles terminated by carboxyl groups (sicastar®, micromod Partikeltechnologie GmbH) were diluted by DI water into 0.1 to 10 wt%. The silica particles with the diameters of 500, 800, 1000, and 1500 nm were used. The colloidal solution of silica particles was stirred with DI water in a homogenizer (Digital Sonifier BRANSON) for 30 minutes. The deposition of silica particles was carried out by the following two-step method. At the first step, 100 µL of this solution was deposited on the c-Si substrate to fully bond the carboxyl groups on the silica particles to the amino groups on the Si substrate for 10 minutes. The adsorbed silica particles on the c-Si substrate work as the trigger of the adsorption of silica particles during the second step. At the second step, the solution was spin-coated on the c-Si substrates at 200 rpm for 10 seconds and dried at 1000–8000 rpm for 30 seconds. The substrates were etched by reactive ion etching (RIE; Samco RIE-10NR). During the RIE, the silica particles work as an etching mask. The flow rates of CF_4 and O_2 were 80 and 8 sccm, respectively. Plasma power was kept constant at 100 W. The etching time (t_{et}) was varied from 3 to 25 minutes. The substrate was immersed in 5% hydrofluoric acid for 1 minute to remove the remaining silica particles. The structures of fabricated molds were observed by scanning electron microscopy (SEM; JEOL JSM-7001F).

The implementation process of LTSs on the back side of c-Si/ITO substrates is shown in Fig. 1(b). The sample size was 1.7 × 1.7 cm^2. 100 nm-thick indium tin oxide (ITO) layer was deposited onto mirror-polished Si substrates by radio-frequency (RF) magnetron sputtering. A master mold was transferred to a soft mold by thermal nanoimprinting. The pressure, temperature, and duration were 0.6 MPa, 130 ^oC, and 1 minute, respectively. A primer (mr-APS-1, microresist technology GmbH) was applied to the specimens by spin coating to improve the release from the soft mold. The rotational speed was increased at a constant slope for 60 seconds and was kept at 5000 rpm for 60 seconds. After natural drying for 5 minutes, an UV curable resin (mr-NIL 210, microresist technology GmbH) was deposited by spin coating. Rotation speeds at the first and second steps were 500 rpm for 30 seconds and 3000 rpm for 25 seconds, respectively. The thickness of the resin was about 100 nm. The soft mold pattern was transferred to the resin by UV nanoimprinting. The pressure and duration were 0.2 MPa and 1 minute, respectively. As shown in Fig. S1, under this nanoimprinting conditions, the morphology of the master mold was successfully transferred to the sample. Silver and aluminum electrodes were deposited on the LTSs. For optical evaluation, the light was incident from the front side of the c-Si/ITO/LTSs/Electrode structure.

Reflectance was measured by a spectrophotometer (Jasco V-570). The short-circuit current density (J_{sc}) was calculated from the reflectance spectra and AM1.5G spectra.

Results And Discussion

Figure 2 shows the silica coverage at five points on the substrate when the silica concentration was varied from 0.1 to 10 wt%. The particle size was 800 nm and the rotation speed was fixed at 8000 rpm. The silica coverage represents the area fraction of the area of adsorbed silica particles to that of Si substrates and calculated from SEM images as shown in Fig. S2. The silica coverage was increased with increasing the silica concentration until 7.5 wt% at all the points. The silica coverage started to saturate at the concentration above 7.5 wt%. This is because at a concentration of 7.5 wt% or higher, a monolayer of silica particles was formed almost all over the substrate by spin coating, and excess silica particles could not reach vacancies and were blown away with the solvent. Although the silica coverage at the center of the substrate was slightly higher than that at the other positions, the silica coverage was generally almost uniform, suggesting that the appropriate rotation speed was set for the uniform deposition.

Figure 3 shows the effect of rotation speed during spin coating on silica coverage. The particle size was 800 nm, and the rotation speed was varied from 1000 to 8000 rpm. The silica solution concentration was 0.1 wt%. The spin coating process is divided into two stages: the first stage is a low-speed process to spread the silica solution uniformly across the substrate, and the second stage is a process to remove the remaining silica solution. Here, the effect of the rotation speed at the second stage on silica coverage was investigated. As the rotation speed was increased, the silica coverage was also increased monotonically. At low rotation speeds, centrifugal force is small and the effect of intermolecular force between silica particles is large. Since the migration distance of silica particles is short, the probability for silica particles to adsorb on the Si substrate could be high. As the rotation speed was increased, the migration distance of silica particles was increased by increasing the centrifugal force. Therefore, the probability for silica particles to adsorb on the Si substrate was increased and the silica coverage was increased. From this result, the rotation speed of 8000 rpm was adopted.

Figure 4 shows the effect of the size of silica particles on silica coverage. Four silica particle sizes of D = 500, 800, 1000, and 1500 nm were used. The rotation speed and the concentration of the silica solution were 8000 rpm and 0.1 wt%, respectively. The silica coverage was increased with increasing silica particle size. Silica particles on a silicon substrate are subject to centrifugal force, convective force, and capillary force (F_{cap}). Centrifugal force and convective force are related with long-range assembly and F_{cap} is related with short-range assembly. Centrifugal force is proportional to the mass of silica particles. Since larger centrifugal force is applied to larger silica particles, the probability to reach capillary assembled region is increased, leading to higher silica coverage. Convective force is caused by hydrodynamic pressure differences due to wetting thickness variation between spots. The spin coating process causes very fast liquid evaporation due to its high-speed spinning. Thus the vapor pressure is a key parameter when selecting a solvent. Since water has a high vapor pressure, rapid liquid evaporation is caused

during spin coating. Wetting layer thickness variations are rapidly decreased from center to edge regions on the substrate. Consequently, the effect of the convective force is not so large. Capillary force is the force of attraction between particles and is represented by Eq. (1), which is illustrated in Fig. 5 [26–28].

$$F_{cap} = 2\pi\gamma \mathrm{r_c^2}(\sin^2\Psi_c)\frac{1}{L}(1)$$

where, γ is the surface tension of the liquid, r_c is the radius of the three-phase contact line at the particle surface, Ψ_c is the mean meniscus slope angle at the contact line, and L is the interparticle distance. From Eq. (1), capillary force is proportional to r_c^2. r_c is increased with increasing D. Therefore, F_{cap} is increased with increasing D.

Figure 6 shows the height of LTSs on the Si master molds fabricated by silica particles with different diameters. The rotation speed and the concentration of the silica solution were 8000 rpm and 0.1 wt%, respectively. Regardless of D, the height of LTSs has a maximum with respect to t_{et}. As D increases, t_{et} when the height of LTSs becomes maximum (t_{h-max}) increases. Each t_{h-max} for D = 500, 800, 100, and 1500 nm was 5, 15, 15, and 25 minutes, respectively. For D = 500 nm, the maximum height was about 200 nm at t_{et}=5 minutes. On the other hand, at D = 1000 nm, the maximum height is about 550 nm around t_{et}=15 minutes. Figure 7 shows SEM images of LTSs at D = 800 nm and (a) t_{et}=3, (b) 5, (c) 10, (d) 15, (e) 20 and (f) 25 minutes. It can be seen that the structure changes from a dome-shape to a cone-shape at 15 minutes, which corresponds to the t_{h-max}. Around t_{et}=t_{h-max}, silica particles started to disappear on the LTSs. By the absence of etching masks, the LTSs themselves were etched and the shape was changed into conical shape and the height of the LTSs was decreased. Therefore, t_{h-max} depends on the etching selectivity between Si and SiO_2. Etching selectivity is decided by the flow rate of CF_4 and O_2. The higher fraction of oxygen leads to reduce silica etch rates. The etching selectivity was highest at 10% oxygen at 0.63 and decreased slightly with increasing the oxygen fraction. [29]. If etching selectivity was decreased, silica particles would disappear at shorter t and t_{h-max} would be decreased and the height of LTSs would be also decreased.

Figure 8 shows the reflectance spectra of LTSs fabricated by silica particles with different diameters at t_{et}=3 minutes. At t_{et}=3 minutes, the height of LTSs was about 100 nm for all the diameters. In the wavelength range from 1000 to 1200 nm, the reflectance is significantly influenced by the reflection on the back side, since the Ag/Al electrode was deposited on the back side. “Ref” shows the reflectance spectra of the structure of c-Si/ITO/Electrode. The nearly 100% reflectance was measured in infrared light range due to back reflection at the rear electrode and low absorption coefficient of Si. The LTSs reduced the reflectance in all the wavelengths compared to the flat sample. The reflectance at 1200 nm was reduced from 98.9 to 81.3% by the LTS with D = 800 nm. The LTSs scattered light and the optical path of the light in the c-Si substrate was increased, leading to the increase in light absorption and the decrease in the reflectance. The reflectance became the lowest at D = 500 and 800 nm. This suggests that there is an optimum aspect ratio of LTSs to reduce the reflectance. Sei *et al*. showed by finite-difference time

domain (FDTD) simulation that the incident light is scattered the most effectively by Si LTSs with a diameter of 700 nm [13]. Sai *et al*. have studied the light-trapping effect of submicron pyramid textures by numerical simulations and showed that an enhanced light-trapping effect occurs because of submicron textures, especially those of similar sizes, as mentioned above [30]. Therefore, the result that D = 500 and 800 nm are optimal for LTSs corresponds to the previous results.

Figure 9 shows the reflectance spectra of LTSs fabricated by silica particles with D=(a) 500, (b) 800, (c) 1000, and (d) 1500 nm. The t_{et} was varied from 3 to 25 minutes. “Ref” shows the reflectance spectra of the structure of c-Si/ITO/Electrode. At all etching times, the reflectance was lower than that of the Ref sample and the lowest reflectance of 81.4% at 1200 nm was obtained at D = 800 nm and t_{et}= 5 minutes. This result corresponds to the previous results. Besides, there is the t_{et} when the reflectance was reduced locally in the whole range (t_{r-min}) for each D. Each t_{r-min} for D = 500, 800, 1000, and 1500 nm was less than 5, 5, 20, and 20 minutes, respectively. Except for D = 1000 nm, t_{r-min} is less than t_{h-max}. One possibility to explain this is the effect of the shape of LTSs. After the height became maximum at t_{h-max}, the shape of LTSs was changed from a dome-shape into a cone-shape. This indicates that the dome-shaped LTSs may be preferable for light scattering compared to cone-shaped LTSs. Another possibility is the effect of silica coverage. The silica coverage was increased with increasing D as shown in Fig. 4. The results in Fig. 9 can be divided into two group; low silica coverage group (G1) and high silica coverage group (G2). D = 500 and 800 nm belong to G1 and D = 1000 and 1500 nm belong to G2. In the case of G1, the silica coverage is low. The scattering effect of a single dome-shaped LTS becomes important. In the case of G2, the silica coverage is high. In this case, the cone-shaped LTS assembly has high scattering effect which is similar to a random pyramid texture. In this way, there is a possibility that light scattering is complicatedly determined by a combination of not only height but also shape and coverage of LTSs.

The projected J_{sc} (pJ_{sc}) was calculated by the reflectance spectra shown in Fig. 8. The pJ_{sc} was calculated by the following equation,

$$pJ_{sc} = \int_{1000\,\mathrm{nm}}^{1200\,\mathrm{nm}} qAN_{photon}d\lambda \quad (2)$$

Where q is the elementary charge, λ is the wavelength of incident light, A is the absorptance, and N_{photon} is the number of photons in AM1.5 G spectrum. Figure 10 shows the increment of pJ_{sc} against the Ref sample (ΔpJ_{sc}). The pJ_{sc} was improved compared to the Ref sample at all D and t_{et}. When t_{et} was short, ΔpJ_{sc} was higher at smaller diameter. On the other hand, when t_{et} was long, ΔpJ_{sc} was higher at larger diameter. This suggests ΔpJ_{sc} was increased when the height of LTSs was lower regardless of the diameter. A maximum gain of 1.00 mA/cm^2 was observed at D = 800 nm and t_{et}=5 min, suggesting that D = 800 nm may be the optimal width for near-infrared light in the 1000 to 1200 nm range and lower aspect ratio is preferable.

Finally, the effect of silica coverage on the reflectance was investigated. Figure 11 shows reflectance spectra for each silica coverage. D = 800 nm, rotation speed = 8000 rpm, and t_{et}=5 minutes were adopted.

Silica coverages of 20, 40, 60% were tuned by the silica concentrations of 0.5, 2.5 and 10 wt%, respectively. The samples were transferred from master molds with silica coverage of 20, 40 and 60%. Actually, the silica coverage transferred to the samples was 16, 45, and 57%, respectively. As shown in Fig. 11, for each silica coverage, the decrease in reflectance was observed with increasing silica coverage and Reflectance increased again when silica concentration exceeded 40%. Figure 12(a), (b), and (c) show SEM image of the samples with the silica coverage of 20, 40, and 60%. Based on the reflectance results, we estimate that the optimum silica coverage to promote light absorption is about 50%. We believe that this is the optimum coverage, where the convexity and concavity by the silica particles are the same. Based on the reflectance results, the highest ΔpJ_{sc} was calculated to be 1.55 mA/cm^2 when the silica coverage was 40%. This leads to the significant contribution to the improvement of J_{sc} in thin crystalline silicon solar cells.

Conclusion

Submicron-sized LTSs were fabricated by a nanoimprint method. Before nanoimprinting, master molds with submicron-sized patterns were prepared by silica colloidal lithography and reactive ion etching. By controlling silica coverage, t_{et} and D, the density, height, and size of LTSs could be controlled. Regardless of D, the height of LTSs has a maximum with respect to t_{et}. As D increases, the t_{et} when the height of LTSs becomes maximum (t_{h-max}) increases. The SEM image revealed that the LTSs were changed from a dome-shape to a cone-shape around t_{et}=t_{h-max}. Around t_{et} =t_{h-max}, silica particles started to disappear on the LTSs. By the absence of etching masks, the LTSs themselves were etched and the shape was changed and the height of the LTSs was decreased. The reflectance of c-Si/ITO/LTSs/Electrode structure was evaluated by spectrophotometer. The reflectance measurement showed that the LTSs reduced the reflectance in the wavelength range from 1000 to 1200 nm compared to the sample without LTSs. This indicates that the fabricated LTSs exhibit optical confinement performance. The ΔpJ_{sc} was calculated from the measured reflectance. Lower aspect ratio leads to higher ΔpJ_{sc}. A maximum gain of 1.00 mA/cm^2 was observed at D = 800 nm and t_{et} =5 minutes, suggesting that D = 800 nm may be the optimal width for the near-infrared light in the range from 1000 to 1200 nm. Furthermore, optimization of the surface coverage resulted in improved short-circuit current density up to 1.55 mA/cm^2. This leads to the significant contribution to the improvement of J_{sc} in thin crystalline silicon solar cells.

Abbreviations

VIPV
Vehicle-integrated photovoltaics
LTS
Light trapping structure
D
Diameter of silica particles

t_{et}
Etching time
c-Si
Crystalline Si
ZnO
Zinc oxice
ITO
Indium tin oxide
RF
Radio-frequency
DI
Deiozied
J_{sc}
Short-circuit current density
F_{cap}
Capillary force
t_{h-max}
t_{et} when the height of LTSs becomes maximum
FDTD
Finite-difference time domain
Ref
Reflectance spectra of the structure of c-Si/ITO/Electrode
t_{r-min}
t_{et} when the reflectance was reduced locally in the whole range
G1
Low silica coverage group
G2
High silica coverage group
pJ_{sc}
projected J_{sc}
ΔpJ_{sc}
Increment of pJ_{sc} against the Ref sample

Declarations

Acknowledgment

This work was supported in part by the New Energy and Industrial Technology Development Organization (NEDO) under the Ministry of Economy Trade and Industry of Japan and Nagoya University Research Fund.

Funding

The study is partially supported by Nagoya University Research Fund and the New Energy and Industrial Technology Development Organization (NEDO) under the Ministry of Economy Trade and Industry of Japan.

Availability of Data and Materials

All data supporting the conclusions of this article are included within the article.

Author's contributions

Yuto Kimata carried out experiment and initial draft of the manuscript. Kazuhiro Gotoh and Shinya Kato supported and advised our experiment. Yasuyoshi Kurokawa and Noritaka Usami gave the final approval of the version of the manuscript to be published. All authors read and approved the final manuscript.

Competing interest

The authors declare that they have no competing interests.

References

1. M. Yamaguchi, K. Araki, K.-H. Lee, N. Kojima, T. Masuda, K. Kimura, A. Satou, and H. Yamada, Proc. the 5th IEEE Int. Conf. on Smart Energy Grid Engineering, 2017, pp. 394.
2. M. Yamaguchi, T. Masuda, K. Araki, D. Sato, K.-H. Lee, N. Kojima, T. Takamoto, K. Okumura, A. Satou, K. Yamada, T. Nakado, Y. Zushi, Y. Ohshita, M. Yamazaki, Prog. Photovoltaics, 29 (2021) 684.
3. M. Yamaguchi, T. Masuda, K. Araki, D. Sato, K.-H. Lee, N. Kojima, T. Takamoto, K. Okumura, A. Satou, K. Yamada, T. Nakado, Y. Zushi, M. Yamazaki, H. Yamada, Energy Power Eng, 12 (2020) 375.
4. M. Yamaguchi, R. Ozaki, K. Nakamura, K. Lee, N. Kojima, Y. Ohshita, T. Masuda, K. Okumura, A. Satou, T. Nakado, K. Yamada, K. Araki, Y. Ota, K. Nishioka, T. Takamoto, Y. Zushi, T. Tanimoto, C. Thiel, A. Tsakalidis, A. Jäger-Waldau, Sol. RRL, 2022, Article 2100429.
5. P. Schygulla, R. Müller, D. Lackner, O. Höhn, H. Hauser, B. Bläsi, F. Predan, J. Benick, M. Hermle, S. W. Glunz, and F. Dimroth, Progress in Photovoltaics: Research and Applications, 30 (2022) 869.
6. Eike Köhnen, Philipp Wagner, Felix Lang, Alexandros Cruz, Bor Li, Marcel Roß,Marko Jošt, Anna B. Morales-Vilches, Marko Topiˇc, Martin Stolterfoht, Dieter Neher,Lars Korte, Bernd Rech, Rutger Schlatmann, Bernd Stannowski,and Steve Albrecht, Solar RRL, 5 (2021) 2100244.
7. H. Sai, T. Oku, Y. Sato, M. Tanabe, T. Matsui, and K. Matsubara, Progress in Photovoltaics, 27 (2019) 1061.
8. W. L. Bailey, M. G. Coleman, C. B. Harris, and I. A. Lesk, US Patent 4137123 (1979).
9. A. Wang, J. Zhao, and M. A. Green, Applied Physics Letter, 57 (1990) 602.

10. J. Zhao, A. Wang, X. Dai, M. A. Green, and S. R. Wenham, Proc. the 22nd IEEE Photovoltaic Specialists Conference, 1991, pp. 399.
11. Y. Kurokawa, O. Aonuma, T. Tayagaki, I. Takahashi, and N. Usami, Japanese Journal of Applied Physics, 56 (2017) 08MA02.
12. A. Hombe, Y. Kurokawa, K. Gotoh, S. Akagi, Y. Yamamoto, D. Yurasov, A. Novikov, and N. Usami, Japanese Journal of Applied Physics, 57 (2018) 08RF09.
13. M. Sei, Y. Kurokawa, S. Kato, and N. Usami, Japanese Journal of Applied Physics, 57 (2018) 08RB21.
14. Y. Ota, A. Hombe, R. Nezasa, D. Yurasov, A. Novikov, M. Shaleev, N. Baidakova, E. Morozova, Y. Kurokawa, and N. Usami, Japanese Journal of Applied Physics, 57 (2018) 08RB04.
15. H. Hauser, A. Mellor, A. Guttowski, C. Wellens, J. Benick, C. Müller, M. Hermle, and B. Bläsi, Energy Procedia, 27 (2012) 337.
16. C. Trompoukis, O. E. Daif, V. Depauw, I. Gordon, and J. Poortmans, Applied Physics Letter, 101 (2012) 103901.
17. A. Mellor, H. Hauser, C. Wellens, J. Benick, J. Eisenlohr, M. Peters, A. Guttowski, I. Tobías, A. Martí, A. Luque, and B. Bläsi, Optics Express 21 (2013) A295.
18. E.-C. Wang, S. Mokkapati, T. P. White, T. Soderstrom, S. Varlamov, and K. R. Catchpole, Progress in Photovoltaics: Research and Applications 22 (2014) 587.
19. N. Tucher, J. Eisenlohr, H. Hauser, J. Benick, M. Graf, C. Müller, M. Hermle, J. C. Goldschmidt, and B. Bläsi, Energy Procedia, 77 (2015) 253.
20. A. Peter Amalathas and M. M. Alkaisi, Materials Science in Semiconductor Processing 57 (2017) 54.
21. D. Liu, Q. Wang, and Q. Wang, Applied Surface Science 439 (2018) 168.
22. H. Hauser, K. Mühlbach, O. Höhn, R. Müller, S. Seitz, J. Rühe, S. W. Glunz, and B. Bläsi, Optics Express, 28 (2020) 10909.
23. S. Kato, Y. Watanabe, Y. Kurokawa, A. Yamada, Y. Ohta, Y. Niwa, and M. Hirota, Japanese Journal of Applied Physics, 51 (2012) 02BP09.
24. W. W. Wenas, A. Yamada, M. Konagai, and K. Takahashi, Japanese Journal of Applied Physics, 30, (1991) L441.
25. A. Hongsingthong, T. Krajangsang, I. A. Yunaz, S. Miyajima, and M. Konagai, Applied Physics Express, 3 (2010) 051102.
26. Jea-Young Choi, T. L. Alford, and Christiana B. Honsberg, Langmuir, 30 (2014) 5732.
27. N. Denkov, O. Velev, P. Kralchevski, I. Ivanov, H. Yoshimura, and K. Nagayama, Langmuir, 8 (1992) 3183.
28. P. A. Kralchevsky, V. N. Paunov, I. B. Ivanov, and K. Nagayama, Journal of Colloid and Interface Science, 151 (1992) 79.
29. See-Eun Cheon, Hyeon-seung Lee, Jihye Choi, Ah Reum Jeong, Taek Sung Lee, Doo Seok Jeong, Kyeong-Seok Lee, Wook-Seong Lee, Won Mok Kim, Heon Lee and Inho Kim. Scientific reports, 7 (2017) 7336.

30. H. Sai, Y. Kanamori, K. Arafune, Y. Oshima, and M. Yamaguchi, Prog. Photovoltaics, 15 (2007) 415.

Figures

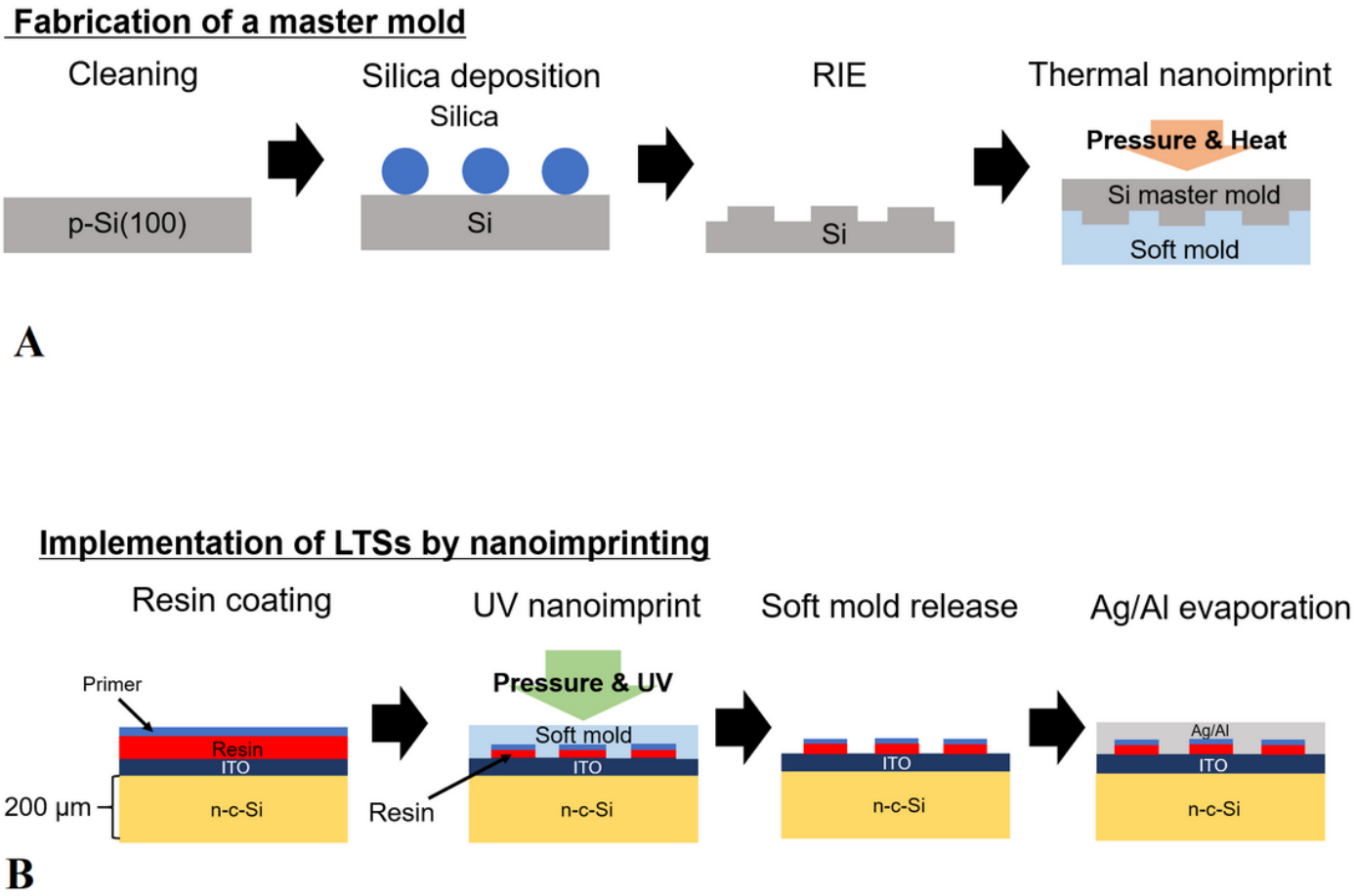

Figure 1

Schematic diagram of (a) the fabrication process of a master mold for LTSs and (b) implementation process of LTSs on a back side ofa solar cells by nanoimprinting.

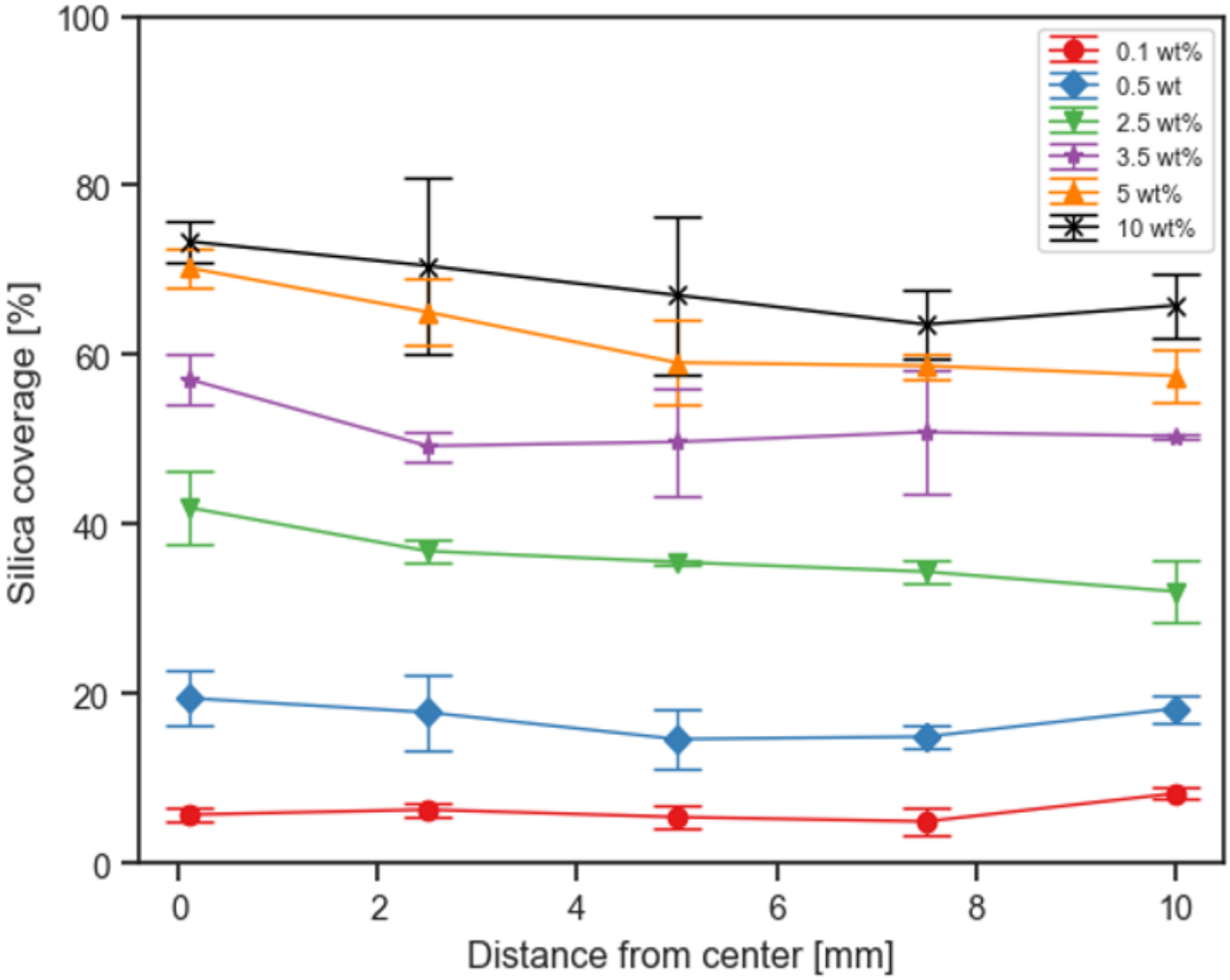

Figure 2

Silica coverage at each point from the center to edge of the substrate. The particle size was 800 nm and the rotation speed was fixed at 8000 rpm. The silica coverage represents the area fraction of the area of adsorbed silica particles to that of Si substrates and was calculated from SEM images as shown in Fig. S2.

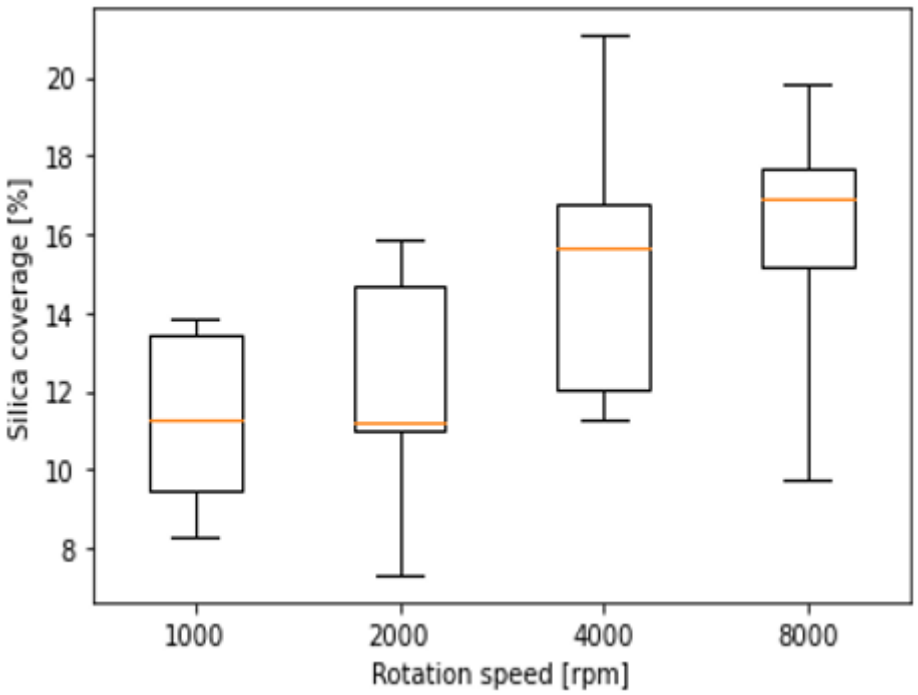

Figure 3

Dependence of silica coverage on rotation speed of spin-coating at the second stage. The silica concentration was varied from 0.1 to 10 wt%. The particle size was 800 nm and the silica solution concentration was 0.1 wt%.

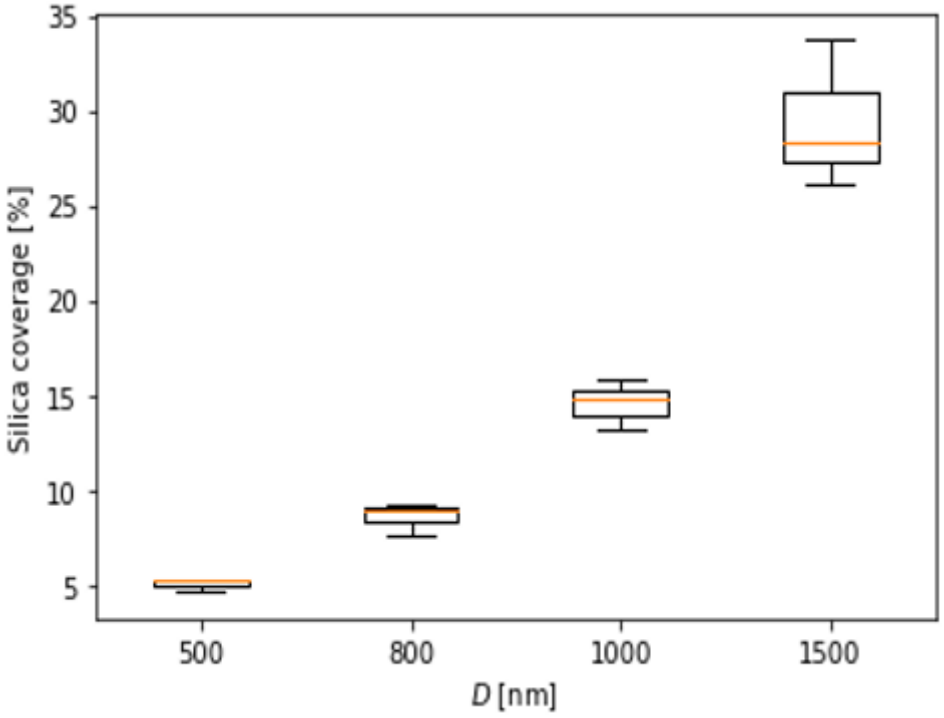

Figure 4

Dependence of silica coverage on *D*. The rotation speed and the concentration of the silica solution were 8000 rpm and 0.1 wt%, respectively.

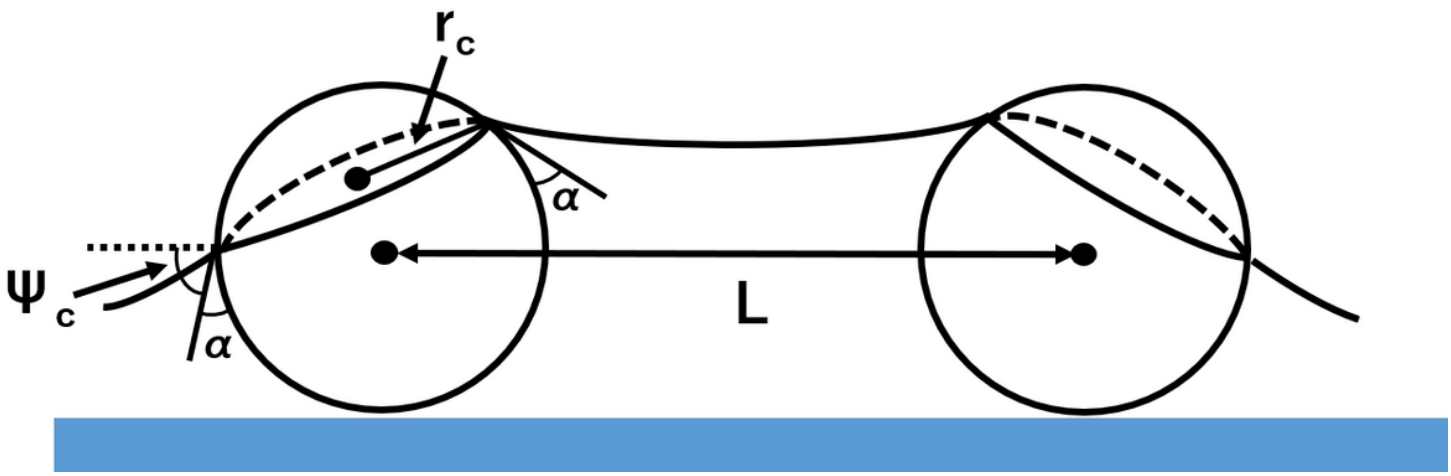

Figure 5

Schematic illustration of two particles partially immersed in a liquid layer for capillary attraction.

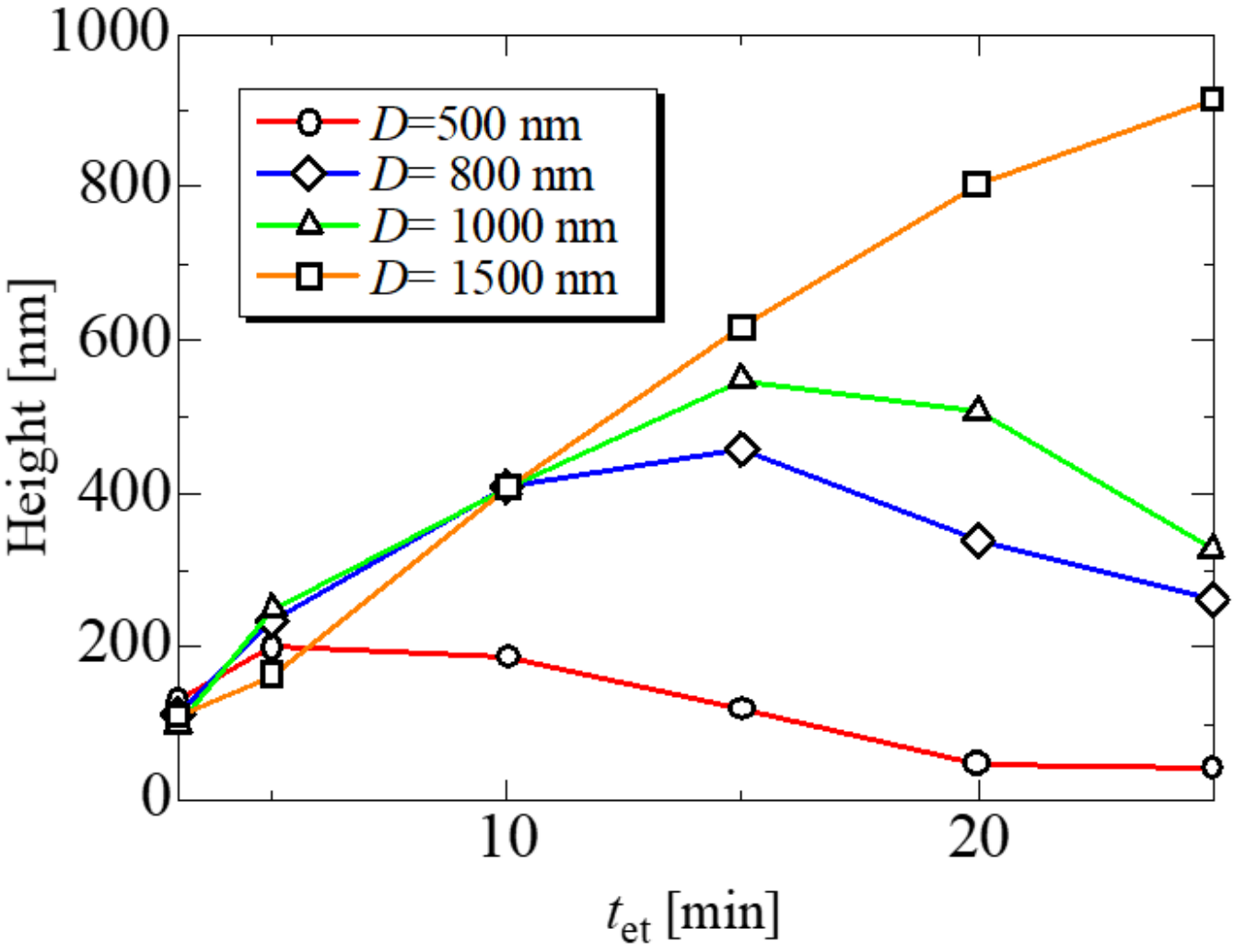

Figure 6

Etching time dependence of the LTS height fabricated by silica particles with a different diameter.

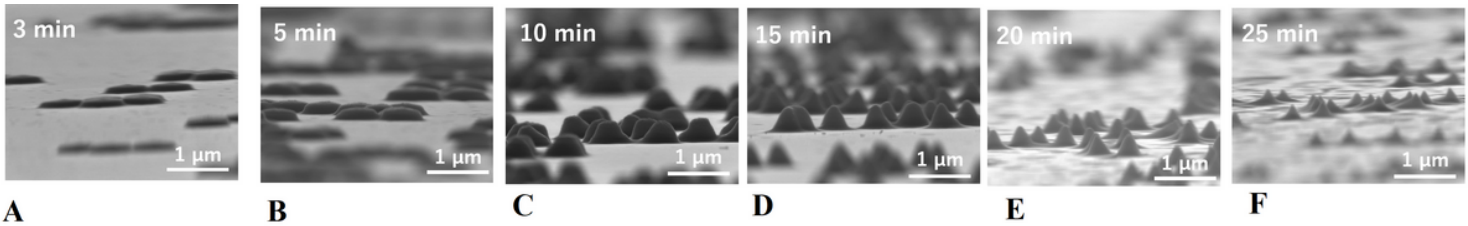

Figure 7

SEM images of LTSs on a master mold fabricated by (a) *D*=800 nm, *t*=3 minutes, (b) *D*=800 nm, *t*=5 minutes, (c) *D*=800 nm, *t*=10 minutes, (d) *D*=800 nm, *t*=15 minutes, (e) *D*=800 nm, *t*=20 minutes, (f) *D*=800 nm, *t*=25 minutes.

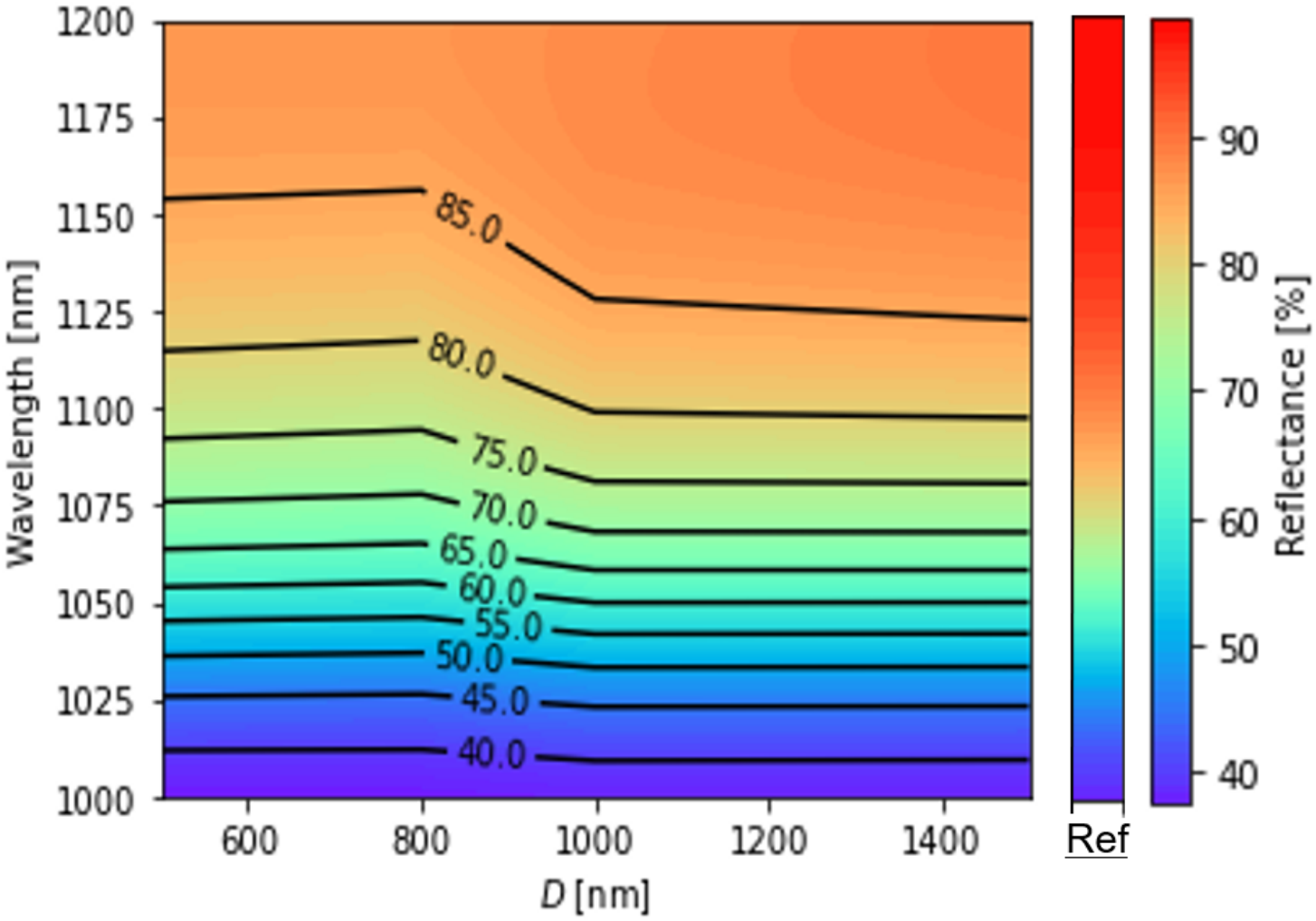

Figure 8

Color mapping of reflectance spectra of LTSs fabricated by silica particles with different D at t_{et}=3 minutes. “Ref” shows the reflectance spectra of the structure of c-Si/ITO/Electrode.

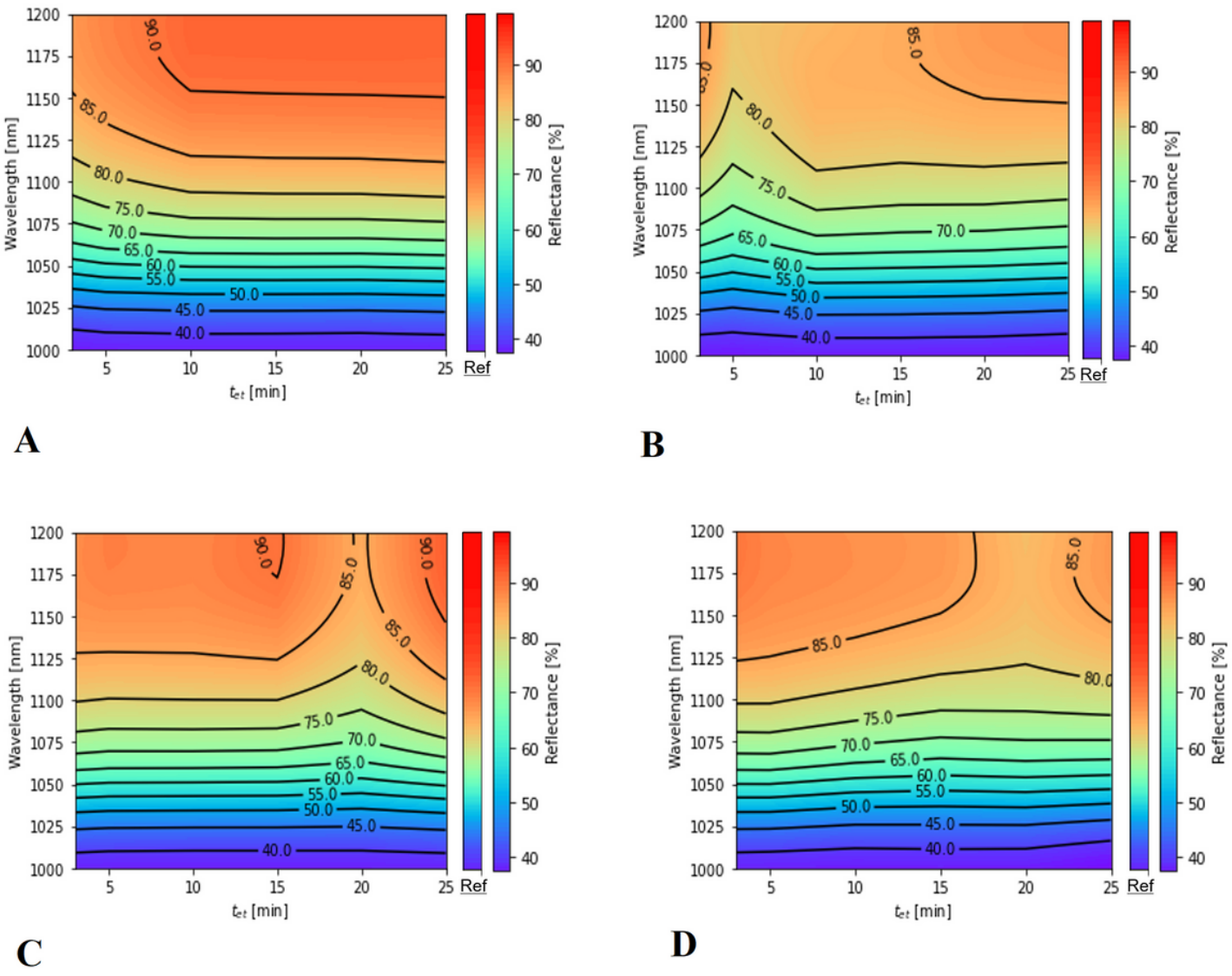

Figure 9

Color mapping of reflectance spectra of LTSs fabricated by silica particles with (a) *D*=500 nm, (b) *D*=800 nm, (c) *D*=1000 nm, (d) *D*=1500 nm. “Ref” shows the reflectance spectra of the structure of c-Si/ITO/Electrode.

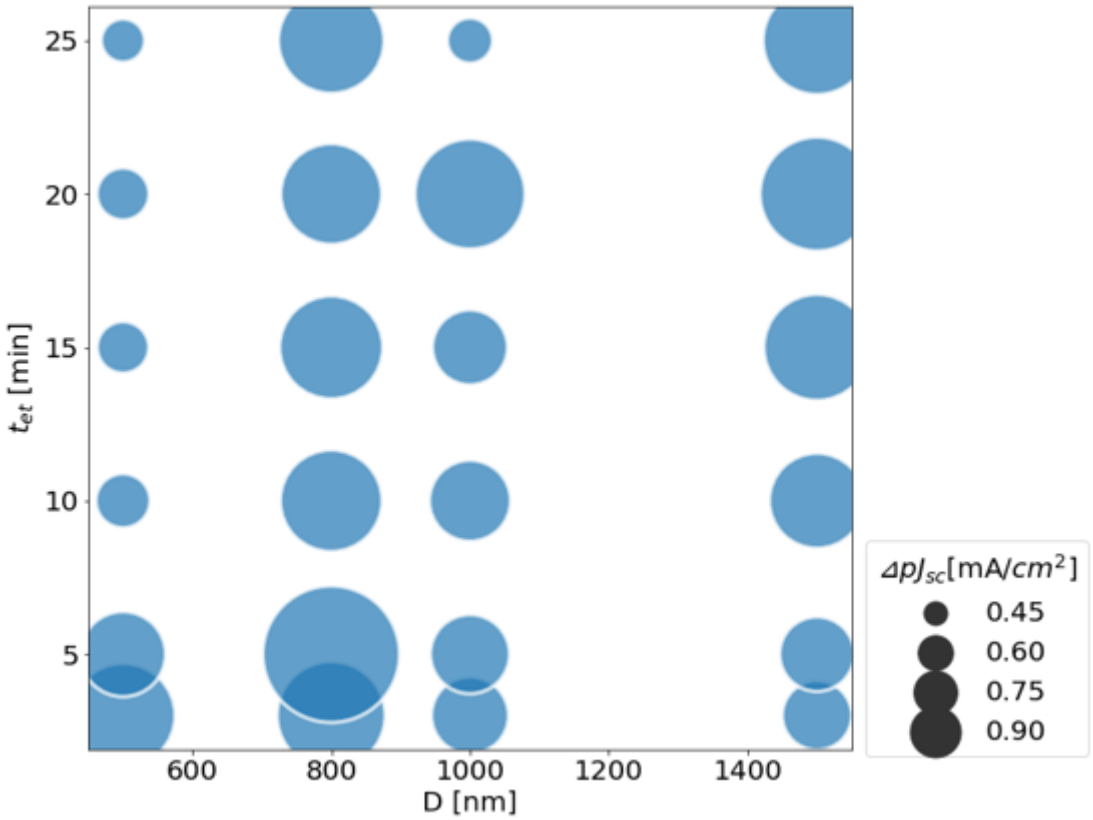

Figure 10

ΔpJ_{sc} calculated from the reflectance spectra shown in Fig. 11 and Eq. (1) as a function of t_{et} and D. The area of each circle represents the absolute value of ΔpJ_{sc}.

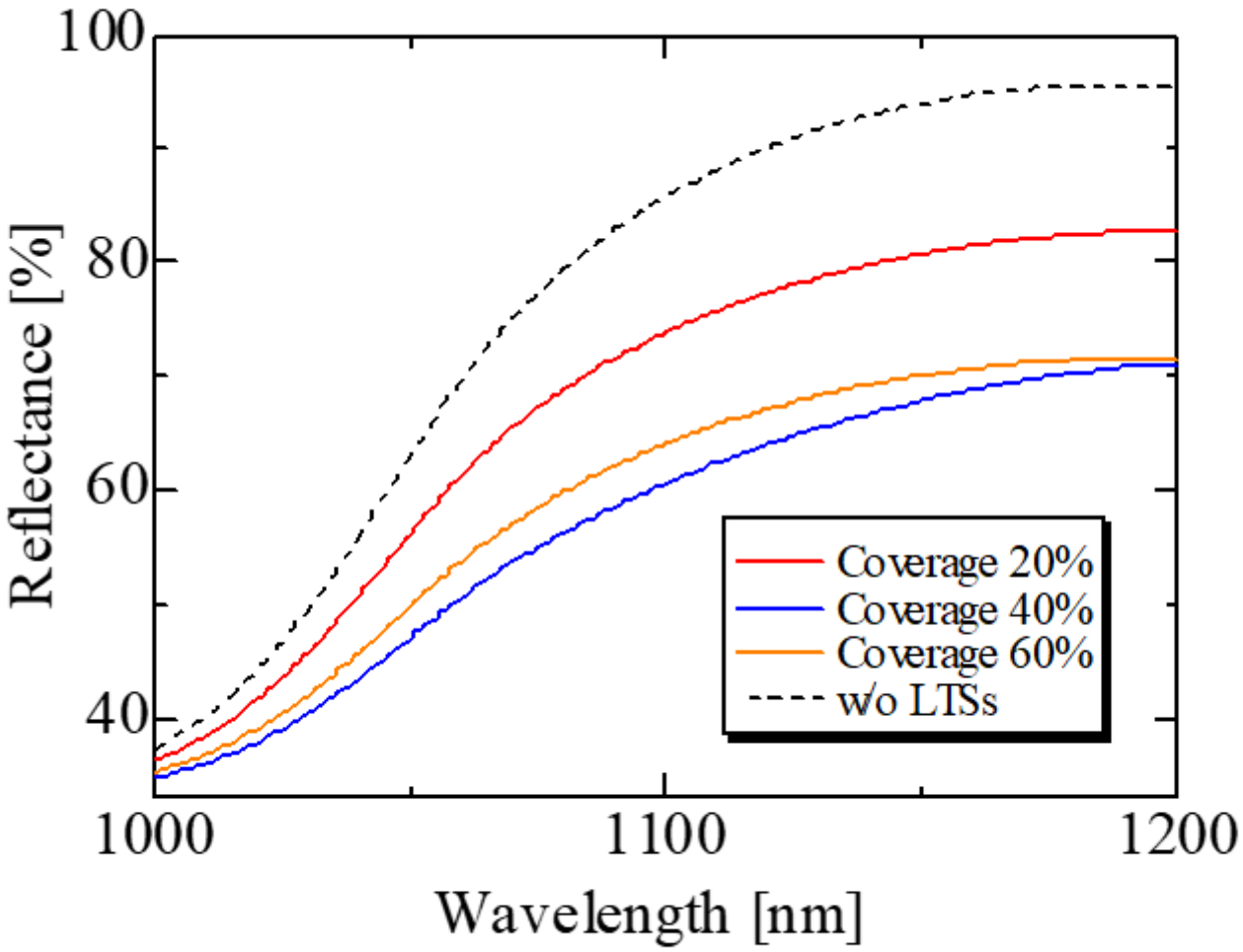

Figure 11

Reflectance spectra of LTSs fabricated by different silica coverages. *D*=800 nm, rotation speed=8000 rpm, and t_{et}=5 minutes were adopted. Silica coverages of 20, 40, 60, and 80% were tuned by the silica concentrations of 0.5, 2.5, 3.5, and 10 wt%, respectively.

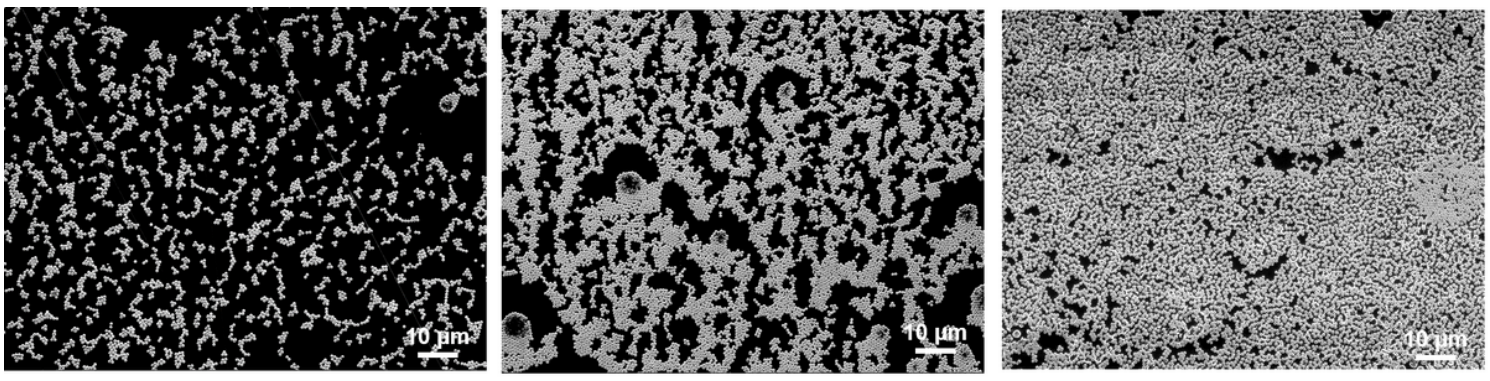

Figure 12

SEM images of silica particles on a silicon substrate with the silica coverage of (a) 20, (b) 40, (c) 80%.

Supplementary Files

This is a list of supplementary files associated with this preprint. Click to download.

- KimataSupplementaryinformation.docx